ACOUSTIC TOMOGRAPHY FOR QUALITATIVE NONDESTRUCTIVE EVALUATION (QNDE) OF STRUCTURAL CONCRETE USING A NEW ULTRASONIC SCANNER SOURCE

Farrokh Jalinoos, Larry D. Olson, Marwan F. Aouad
Olson Engineering
14818 W. 6th Ave, #5A
Golden, CO 80401

A. H. Balch
Department of Geophysics
Colorado School of Mines
Golden CO, 80401

INTRODUCTION

Civil engineers have used Nondestructive Testing and Evaluation (NDT&E) methods based on Ultrasonic Pulse Velocity (UPV) measurements as far back as the 1940's to evaluate the condition of new construction and monitor the integrity of the existing infrastructure. A major emphasis in concrete NDT is the evaluation of concrete integrity and the detection of defects such as voids, honeycomb, cracking, and delamination in concrete. The conventional UPV tests (ASTM Standard C597-83) may indicate the presence of a flaw, but are limited in determining the depth (but not the lateral definition) of the flaw. The commercially available UPV systems all use point-by-point measurement approaches that are too slow to economically gather enough information to create images of internal conditions for large concrete areas.

Over the past 100 years, many imaging techniques have been developed including X-ray, acoustical, radar, infrared, Nuclear Magnetic Resonance, Biomedical Computed Tomography, and so forth. Recent improvements in computer technologies and data acquisition systems make possible the economical utilization of signal processing and reconstruction imaging techniques from the medical, geophysical and aerospace industries. In the construction industry, however, relatively few imaging technologies have been developed for reinforced concrete. A tomogram in a concrete structure has heretofore been impractical due to its prohibitive cost and time required. Thus, the scanner system was developed specifically to increase the data acquisition speed for the Ultrasonic Pulse Velocity (UPV) testing method and to provide information on the closely-spaced grid that is required for imaging purposes.

Review of Progress in Quantitative Nondestructive Evaluation, Vol. 14
Edited by D.O. Thompson and D.E. Chimenti, Plenum Press, New York, 1995

THEORY

Cross-medium tomography involves imaging of the sonic properties of a specimen from the observation of the transmitted compressional or shear first arrival energy. A line integral relationship exists between sonic velocity field v(x,y) (or similarly attenuation) and travel time t_i (or amplitude), for a ray i, and is given by:

$$t_i = \int_{Ri} ds / v(x,y) \qquad (1)$$

where R_i denotes the curve connecting a source receiver pair which yields the least possible travel time according to Fermat's principle. Note that Equation (1) is a high frequency approximation and t is a non-linear functional of the velocity parameter due to the complex dependence of R_i on velocity v(x,y). Cross-medium tomography is an attempt to match model responses (calculated travel times) to observed data by inversion of these line integrals. With a suitable choice of slowness space (1/v), the functional t_i becomes Fréchet differentiable and thereby we can use linear approximations. The region of interest is divided into rectangular grid of cells (j), with a constant v on each cell. A discrete approximation of the line integral can be written as:

$$t_i = \sum_j \Delta S_{ij} / V_j \qquad (2)$$

where ΔS_{ij} is the distance traveled by ray i in cell j, and V_j velocity within cell j. Using a first order Taylor expansion of the observation O_i and model M_i with respect to model parameters P_j, we derive:

$$O_i = M_i (p^0) + \sum^{M}_{j=1} \partial M_i / \partial P_j \; . \; \Delta p_j \; + \; e_i \qquad (3)$$

where e_i is the residual error. Defining the vector $d_i = O_i - M_i$, for the difference between computed travel times from the model and the field observation, and Δp_j as the difference between the true and the modelled slowness, the Equation (3) can be written in matrix form as:

$$\underline{d} = A \, \underline{\Delta p} \qquad (4)$$

for Jacobian or the sensitivity matrix A and neglecting the residual error $\underline{e}$. In this paper, we have sought to solve (4) by using two series expansion approaches from geotomography: an optimized and efficient matrix inversion approach based on the Conjugate Gradient (CG) inversion technique [4, 5]; and another "backprojection" approach, adapted from medical tomography [2,3] of Simultaneous Iterative Reconstruction Technique (SIRT).

The least square matrix inversion formulation of (4) requires minimization of cumulative squared error of the loss function with respect to parameter change $\underline{\Delta p}$ giving rise to "normal equations":

$$A^T A \, \underline{\Delta p} = A^T \underline{d} \qquad (5)$$

A common solution to Equation (5) incorporates the well-known Marquardt-Levenberg approach given by:

$$\underline{\Delta p} = (A^T A + \lambda I)^{-1} A^T \underline{d} \qquad (6)$$

where λ is the damping constant which adds to the diagonal of A^TA, A^T is the transpose of matrix A, and I is the identity matrix. Damping is used to minimize the ill-conditioning by keeping the eigenvalues in Equation (6) from becoming too small. The matrix A^TA is square, symmetric, and can be singular. For the large and sparse tomographic inversion problem, a conjugate gradient solution to Equation (5), as described by Scales [4,5], was also used in this paper, without the explicit formation of the A^TA matrix.

The SIRT approach is particularly well suited for the typically large and sparse overdetermined A matrix in Equation (4) where the number of observations are greater than the unknown parameters. It seeks a solution one slowness cell at a time:

$$\Delta\alpha_{ij} = d_i x_{ij} / \sum^{M}_{j=1} (x_{ij})^2;$$
$$\Delta p_j = 1/N \sum^{N}_{i=1} \Delta\alpha_{ij} \qquad (7)$$

where $\Delta\alpha_{ij}$ is the correction factor, x_{ij} is the distance of travel of ray i in cell j, d_i is the difference between the observed and calculated travel times, and N is the number of rays intersecting the j^{th} pixel. In this approach, the difference between the computed and observed travel times is treated as an error. This error is backprojected along individual raypaths and the velocity values in the intersecting pixels are adjusted in proportion to the distance travelled through each cell. The velocity corrections are averaged out and applied in the end after all rays have been traced.

The series expansion approach requires the medium between the source and receiver lines to be discretized into a number of constant slowness cells. The sonic wavefield is propagated through the discretized cells and a set of travel times is obtained by ray tracing (forward modelling). In this paper, curved raypaths were computed using a gradient minimization technique. The set of travel time equations is inverted in a manner to reduce the root mean square (RMS) error between the observed and computed travel times. Tomography can be used in inverting both the travel time (velocity tomography) and amplitude (attenuation tomography) data.

SYNOPSIS OF THE TEST RESULTS

In order to study the application of tomography for nondestructive imaging of flaws in concrete, four concrete walls were constructed with honeycombs, simulated voids, simulated cracks, poor quality concrete and steel rebar [6]. The nominal dimensions of the walls were 122x122x30.5 cm (48x48x12 in). Voids were simulated by placing styrofoam into the concrete mix. The honeycombs were built by loosely hand placing concrete in small forms without consolidation prior to concrete placement. Open cracks were simulated by inserting thin sheets of solid cardboard into Ziploc bags and inflating the bags to a thickness of approximately 0.64 cm (1/4 in). The weak concrete was made by adding more water to the original mix. Simulated microcracks were made by inserting one- and two- layer sunscreen mesh into the concrete mix. Three steel bars (numbers 8, 11 and 14) were also placed in one of the walls.

A total of 11 tomographic images were obtained (each utilizing over 1700 data traces) using the rolling UPV scanner source and a 150 kHz James Instruments UPV receiver. The source was excited at its 35 kHz resonant frequency, and the recorded signal was amplified and band-pass filtered between 20-40 kHz. The analog signal was digitized

using a PC-based digital oscilloscope system at a 1 microsecond sampling interval. An example of a picked first arrival travel time and amplitude plot is shown in Fig. 1.

Typical tomographic data collection involves scanning the region of interest along a scan line with many combinations of source and receiver locations. In our tests, the receiver was held constant at a certain elevation on the wall and the source was rolled continuously on the opposite side of the wall. The receiver was then moved to the next survey location and the test was repeated. A typical scan line for the receiver held fixed at the middle of a wall is shown in Fig. 1. The rolling source was water coupled and was pulled using a cable pulley system along the scanned survey line. Grease was used as the couplant for the fixed UPV receiver. Scans were obtained for a total of 42 source and receiver locations, giving rise to 1764 source/receiver measurement combinations (or raypaths) per complete scan. For a 122x122x30.5 cm (48x48x12 in) wall, a typical 116 cm (45.5 in) scan took only 1 1/2 hours to perform (for single channel recording) for 1764 different source-receiver combinations. A comparable test line takes approximately 40-60 hours to perform on a single source-receiver measurement basis. The velocity field between the source and receiver survey line was discretized to 473 cells. Each cell had a dimension of 2.5x2.5 cm (1x1 in). Therefore, in the language of matrix inversion, there were 1764 equations and 473 unknown parameters for this problem.

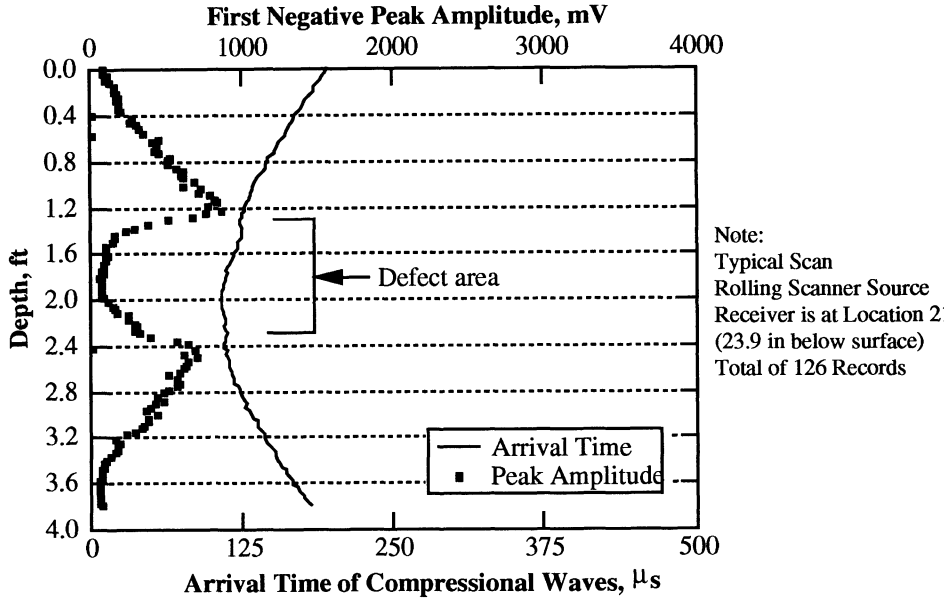

Figure 1. Typical Arrival Time and Peak Amplitude Plots

In addition to the four walls cast-in-place at Olson Engineering, a 1.8x1.8x0.6 m (6x6x2 ft) concrete wall with a 12.7-cm (5-in) diameter horizontal corehole was tested at the Colorado School of Mines (CSM). The survey was initially done to compare the results obtained from the rolling UPV scanner with the point-by-point previous survey results by Dr. Balch and his students of the same wall. Dr. Balch's reflection and diffraction data sets were acquired on a point-by-point basis and took about 2 weeks per survey line. For a 1.2 m (4 ft) survey line, our survey consisted of 25 source and 25 receiver locations for 625 raypaths (or knowns) and it took only 1 1/2 hours to obtain the data. The scan region was discretized into 312 cells (unknown) of 5.1x5.1 cm (2x2 in) in dimension. This initial tomographic survey was thus performed on a much coarser grid than the ones done on the walls constructed at Olson Engineering. Results from our tomographic analysis and the earlier reflection/diffraction imaging performed by Dr. Balch and his students indicated a clear image of the 12.7 cm (5-in) diameter horizontal core in the middle of the CSM wall.

Figure 2 shows a Conjugate Gradient (CG) based velocity tomogram obtained through the 1.2x1.2x0.3-m (4x4x1-ft) thick wall along a scan line that contains two styrofoam voids. The dimensions of the voids are 15.2x10.2 cm (6x4 in, top) and 10.2x10.2 cm (4x4 in, bottom) and are centered at a distance of 30.5 cm (12 in) from the top and the bottom of the wall, respectively. Also shown in Fig 2 are the initial velocity guess and the ray density plots. The bar scale shows velocity in both ft/s and m/s, and the ray density plot indicates number of rays per cell. For the two-sided coverage (equal source/receiver spacing intervals), all ray density plots displayed a characteristic X-pattern for the high ray density zones. Artifacts are more likely to be formed in the low ray density zones where the confidence in the final image is lower. The initial velocity guess was based on the travel time of the compressional waves when the source and receiver were at the same elevation (common offset). The initial guess plays an important role in the image resolution, as tomography works best when the final solution is reasonably close to the initial guess. If the final image indicates anomalous velocity zones outside of those suggested by the initial velocity guess, it may suggest the presence of artifacts.

The locations of the two voids are indicated by the light zones in the velocity tomogram of Fig. 2. Note that the voids were identified even though they were not centered in the middle of the scanned area where the ray density is high. Despite the low to medium ray density coverage, the results show that tomography is effective in detecting small voids on the order of 7.6-10.2 cm (3-4 in) in dimension. Tomography generally results in a smooth, low-velocity contrast image, even though in this case we had a high velocity contrast anomaly. Similar void definition was also obtained by using the PC-based SIRT program.

In the case of honeycomb defects, the velocity-based tomographic analyses imaged only one of the four defects present in the walls. Although the unit weight of the honeycombs was much lower than the unit weight of regular concrete, the difference in ultrasonic pulse velocity was small. Consequently, velocity tomography was ineffective in locating defects with less than 5% velocity contrast from sound concrete. Similarly, velocity tomography failed to image weak concrete. Travel time delays of only 4% were obtained, even though the compressive strength of weak concrete was about 25% lower. More research is needed for studying the influence of varying the percentage of fine grains in the concrete matrix on the ultrasonic velocities for different honeycomb flaws.

Velocity tomography was shown to be a promising tool for studying simulated open to closed cracks. Full image resolution was not obtained by velocity tomography, but crack defect zones were identified. We believe the center of the largest inflated Ziploc bag

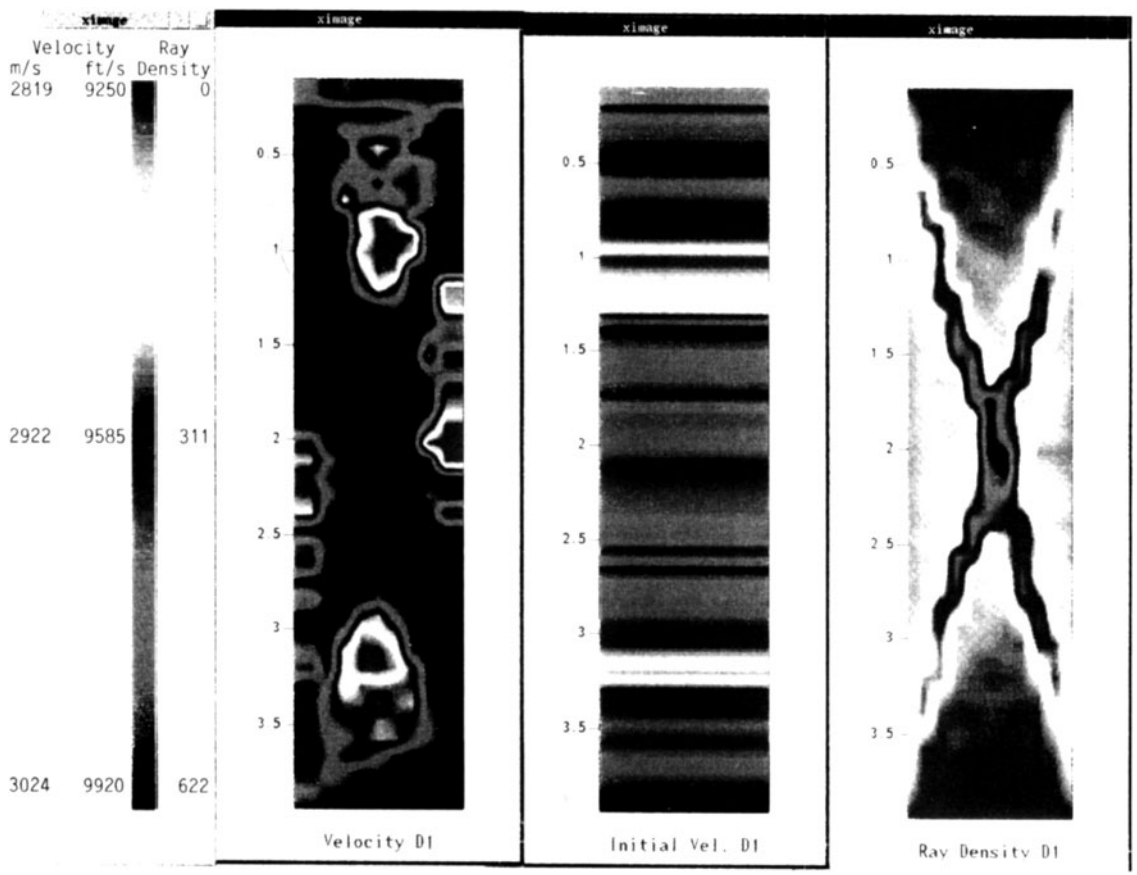

Figure 2. Conjugate Gradient (CG) Based Velocity Tomogram from a Wall Containing Two Simulated Voids.

unfortunately collapsed during the concrete placement. Consequently, the picked travel times and amplitudes did not follow a regular trend due to the random contact conditions across the bag. However, 90% reductions in amplitudes were noted. This resulted in better crack image definition using amplitude tomography than travel time tomography. Thus, amplitude tomography appears to be a better tool for studying closed cracks than velocity tomography. It may also prove to be more effective for honeycomb-type defects. Due to time constraints, P-wave amplitude tomography was only performed on one survey line.

SUMMARY AND CONCLUSIONS

A summary of our findings in Phase I is shown in Table 1 below. As indicated, the travel time velocity tomography was most successful in locating voids in concrete (the voids also had the highest velocity contrast anomaly). Conventional Ultrasonic Pulse Velocity (UPV) tests also showed up to a 10% delay in travel time for void versus sound concrete. Velocity tomography was also effective in identifying the location of the corehole in the Colorado School of Mines (CSM) wall. Evaluation of other defects included honeycombs, simulated open cracks and simulated microcracks. These comparatively small simulated defects indicated velocity reductions of less than or equal to 5% versus sound concrete.

Table 1. Summary of Phase I results.

Type of Defect	*Void*	*Honeycomb*	*Weak Concrete*	*Open Crack*	*Micro-Crack*
Total Time Delay	+10%	+4%	+4%	+5%	+5%
Amplitude Loss	-	-	-	-90%	-
Velocity Tomogram	**G-E**	**F**	**P-F**	**P-F**	**G**
Amplitude Tomogram	-	-	-	**F-G**	-
Degree of Velocity Contrast	High	Low	Low	Medium	Medium-High
Preliminary Assessment of Velocity and Amplitude Tomography	Excellent for V_p, V_s, a_p, a_S	V_s might be better than V_p; V_p better than a_p	V_s might be better than V_p; V_p better than a_p	a_p, a_s might be better than V_p, V_s	a_p, a_s might be better than V_p, V_s

Symbol Keys: **E**: Excellent; **G**: Good; **F**: Fair; **P**: Poor.
V_p: Compressional Velocity Tomogram; V_s: Shear Velocity Tomogram;
a_p: Compressional Attenuation Tomogram; a_s: Shear Attenuation Tomogram

It must be noted that this tomographic inversion method suffers from the problem of non-uniqueness inherent in this procedure. However, non-uniqueness problems can be reduced by designing surveys with large density of rays (specially vertical rays) intersecting each cell.

The results of the Phase I study indicate that the ultrasonic scanner now makes imaging of concrete flaws practical using well known tomographic techniques. This analysis can, therefore, be extended and applied as a diagnostic tool for acoustic imaging of internal flaws in civil concrete structures, such as buildings, bridges, slurry walls, and dams.

ACKNOWLEDGEMENTS

This Phase I research was sponsored by National Science Foundation (NSF) Small Business Innovation Research (SBIR) program. We like to thank NSF for their support in this project.

REFERENCES

1. K. A. Dines and R. J. Lytle, "Computerized Geophysical Tomography", *Proc. IEEE*, Vol 67, (1979), pp. 1065-1073.
2. G. T. Herman, *Image Reconstruction from Projections, the Fundamentals of Computerized Tomography* (Academic Press, Inc., 1980).
3. S. Ivansson, "Seismic Borehole Tomography- Theory and Computation Methods", *Proc. IEEE*, Vol 74, (1986), pp. 328-338.
4. G. Nolet, Seismic Wave Propagation and Seismic Tomography, in *Seismic Tomography with Applications in Global Seismology and Exploration Geophysics*, ed. G. Nolet (D. Reidal Publishing Co., 1987), pp. 1-23.
5. J. A. Scales, "Tomographic Inversion via the Conjugate Gradient Method", *Geophysics*, Vol 52, (1987), pp. 179-185.
6. L. D. Olson, F. Jalinoos, M. F. Aouad, A. H. Balch, " Acoustic Tomography and Reflection Imaging for Nondestructive Evaluation of Structural Concrete, NSF Phase I Final Report (Award # 9260840), SBIR Industrial Innovation Interface Division, Washington D. C., 1993.